Journal of Pharmaceutical Innovation
https://doi.org/10.1007/s12247-020-09508-3

ORIGINAL ARTICLE

Effect of Presence of Aliphatic Glycine in the Anti-cancer Platinum Complex Structure on Human Serum Albumin Binding

Afrooz Shiekhzadeh[1] · Nasrin Sohrabi[1] · Mahboube Eslami Moghadam[2] · Mohsen Oftadeh[1] · Adeleh Divsalar[3]

Accepted: 11 October 2020

Abstract

Purpose In this work, a new water-soluble Pt(II) complex was synthesized with aliphatic glycine ligand with a formula of cis-[$Pt(NH_3)_2$(isopentylgly)]NO_3, as an anti-cancer drug, and characterized. To determine the binding constant of the human serum albumin (HSA, the most abundant carrier proteins in the human circulatory system) to this complex and the binding site of the complex on HSA, the melting point of HSA and the kinetics of this interaction were investigated to introduce an anti-breast cancer drug with fewer side effects.

Methods HSA interaction with the complex was studied via a spectroscopic method at 27 and 37 °C and physiological situation (I = 10 mM, pH = 7.4) and molecular docking.

Results The toxicity value of this complex was obtained against the human cancer breast cell line of MCF-7. The thermodynamic parameters of enthalpy and entropy were also achieved in the empirical procedure. Due to the spontaneity of the interaction, Gibbs free energy variation was obtained negative. The binding constant of this complex to HSA was 3.9×10^5 (M^{-1}). Empirical results showed that the quenching mechanism was static. Hill coefficients, Hill constant, complex aggregation number around protein, number of binding sites, and protein melting temperature with complex were obtained. The kinetics of this interaction was also investigated, which showed that this interaction follows a second-order kinetic. The molecular docking data indicated that the position of the interaction of complex on the protein was the site I in the subsecond IIA. Also, the hydrogen bonding and the hydrophobic interaction as the dominant binding forces were seen in complex–HSA formation.

Conclusion This interaction with positive cooperativity was recognized via a superior hydrogen bond. The reasonable binding constant was also obtained, which could ultimately be a good option as an anti–breast cancer drug.

Keywords Human serum albumin · Hill constant · Aggregation number · Platinum(II) complex · Molecular docking

Abbreviations

HSA Human serum albumin
PDB Protein Data Bank

✉ Nasrin Sohrabi
sohrabnas@pnu.ac.ir; nsohrabi48@gmail.com

✉ Mahboube Eslami Moghadam
eslami_moghadam@ccerci.ac.ir; eslami_moghadam@yahoo.com

[1] Department of Chemistry, Payame Noor University (PNU), P.O BOX 19395-4697, Tehran, Iran

[2] Chemistry & Chemical Engineering Research Center of Iran, Tehran, Iran

[3] Department of cell & molecular biology, Faculty of Biological Sciences, Karazmi University, Tehran, Iran

Introduction

In chemotherapy, the interaction of the anti-cancer metallodrugs with proteins especially human serum albumin (HSA) can affect the biological activity of the body [1]. The study of this significant interaction is very suitable for obtaining information about absorption, distribution, metabolism, and drug excretion [2]. Human serum albumin is used as an important blood carrier protein folding in investigating drug binding to protein [3]. This protein contains a polypeptide chain with 585 amino acids [3]. In 1992, researchers obtained the 3D dimensional structure of HSA via the X-ray crystallographic method [3]. Among proteins, HSA has been studied more than other proteins [2]. The interaction between protein and hydrophobic drugs increases the solubility of the drug in the blood [2]. The interaction of HSA with drugs often leads to a change in the structure of the HSA [3].

Published online: 21 October 2020

Today, the design and synthesis of anti-cancer metallodrugs have been considered and inorganic chemistry has grown dramatically in medicine [4]. The most important side effects of cisplatin, carboplatin, and oxaliplatin are nephrotoxicity, myelosuppression, and neurotoxicity respectively. Due to cisplatin side effects (nausea and vomiting (may be severe), diarrhea, temporary hair loss, inability to taste the food, hiccups, dark urine, dry mouth, decreased sweating, dry skin, and other signs of dehydration), today, research has demonstrated that if chloride ligands in cisplatin structure are replaced by N, O donate chelate ligands such as amines acids, it will become an anti-cancer drug with fewer side effects [5]. It is better if the substituted chloride ligands are more biocompatible and natural (such as glycine). In our proposed complexes, no side effects were observed due to the use of glycine derivatives, which are a body-friendly, non-toxic amino acid. Metal complexes interact with HSA via the coupling of covalent and non-covalent [6]. The metal complexes tend to interact with Trp 214 residue at the surface of the protein, which makes it easier to access them [4]. The interaction between drugs and bio-macromolecules has increased in recent years [7–16]. Several techniques including equilibrium dialysis, fluorescence, absorption spectroscopy, and circular dichroism (CD) have been used to examine the interaction of the complex with bio-macromolecule [17]. The interactions between macromolecule and drugs are mostly shown with spectroscopic techniques as these methods are susceptible and rather easy to use [18].

In this work, a new complex, cis-[Pt(NH_3)$_2$(isopentylgly)]NO_3, was designed, synthesized, and characterized (see Scheme 1). Also, the interaction of HSA with a new soluble complex was studied via UV-Vis, fluorescence, and molecular docking. Then, the enthalpy $\left(\Delta H_b^{\circ}\right)$, entropy $\left(\Delta S_b^{\circ}\right)$, and Gibbs free energy $\left(\Delta G_b^{\circ}\right)$ changes, melting point of HSA with and without Pt-drug, T_m, as well as the aggregation number drug around HSA, <J>, were calculated and the number of binding sites g; binding constants, K_b, Hill coefficient, n_H, Stern–Volmer coefficient, K_{sv}, quenching constant, k_q, and the sort of quenching mechanism were obtained. Afterward, the kinetics of this interaction was investigated. In the theoretical sector, the interaction between HSA and Pt complex was studied using molecular docking. The outcomes showed that the type of HSA binding with Pt complex is hydrogen and hydrophobic interactions.

Experimental

Materials and Methods

Silver nitrate, potassium iodide, isopentyl amine, ammonia, sodium bicarbonate, and potassium tetrachloroplatinate were purchased from Merck (Germany). Acetone, anhydrous diethyl ether, and ethanol were purchased from Merck Co (Germany). Human serum albumin with purity > 99.0% was bought from Sigma-Aldrich Co. (USA), and its solution was prepared 0.03 mM with tris-buffer. The stock solution of the Pt(II) complex (2 mM) was prepared with tris-HCl buffer containing NaCl (10 mM, pH 7.4). Infrared spectra were measured on an FT-IR 8400 Shimadzu spectrometer in the KBr pellets. ^{1}HNMR (300 MHz) spectrum was collected on Bruker BRX-250 Avance spectrometer with reference as DMSO-d_6 solvent. The melting point of the complex was recorded on a Buchi (Flawil, Switzerland) melting point B-545. Conductivity measurement was carried out by using a Tetra Con 325 electrode with a cell constant of 0.951 connected to a Terminal 740 (WTW, Germany). Elemental analysis (C, H, and N) of the complex carried out by a CHN has been analyzed by elementary Analysensysteme Gmb4-Vario EL III.

All fluorescence spectra were performed on a Scinco FS-2 fluorescence spectrophotometer in 200–700 nm. UV spectra of HSA binding studies with various concentrations of Pt(II) complex were measured using the Perkin Elmer Precisely Lambda 25 Spectrophotometer within 200–700 nm.

Synthesis of *cis*-[Pt(NH_3)$_2$(Isopentylgly)]NO_3

Isopentyl glycine was prepared by using the method previously published and used for the synthesis of the complex [5]. Also, $cis-[Pt(NH_3)_2I_2]$ was synthesized according to the approach described previously [19]. Specifically, 0.138 mmol (0.066 g) $cis-[Pt(NH_3)_2I_2]$ and 0.275 mmol (0.047 g) $AgNO_3$ were suspended in 14-mL water under continuous stirring at room temperature for 24 h and refluxed at 50 °C for 30 min under darkness. Then, gray AgI precipitate was removed through centrifugation. Next, the solution of 0.138 mmol (0.025 g) isopentyl glycine hydrochloride and 0.276 mmol (0.023 g) $NaHCO_3$ in 10-mL distilled water was added to the above-centrifuged solution and stirred at 40 °C for 4 h. The solution was concentrated until a brown

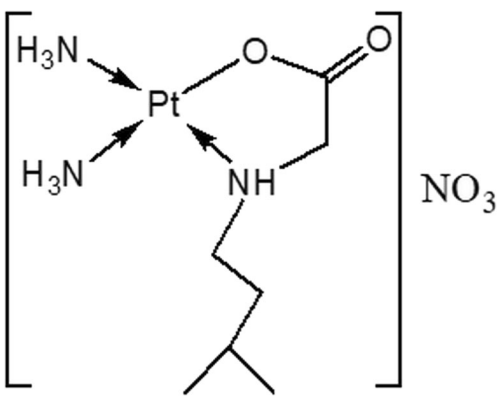

Scheme 1 The proposed structure of the *cis*-[Pt(NH_3)$_2$(isopentylgly)]NO_3 complex

Scheme 2 The general procedure of complex formation

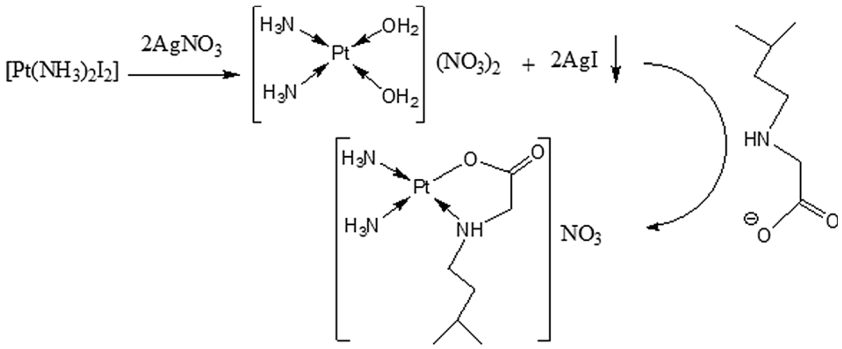

precipitate appeared. The obtained product was filtered and washed with cold acetone and dried in a desiccator. The formation of the complex is shown in Scheme 2. *cis*-$[Pt(NH_3)_2(isopentylgly)]NO_3$: The yield is 71%; analytical calculated for $C_7H_{20}N_3O_2Pt$ compound (435.08 g/mol) is C, 19.30; H, 4.59; N, 9.65%, analytical found: C, 19.11; H, 4.34; N, 9.23%; UV: λ_{max} nm (ε_M): 198 (20.4); molar conductance, (ΛM) of 0.1 mM = 121 Ω^{-1} cm^2 mol^{-1}; mp: 115–125 °C; IR (cm^{-1}, KBr pellet): 3430 (s, N-H), 3271 (s, C-H), 1633 (s, C=O), 1383 (s, $(NO_3)^-$); ^{1}H NMR (300 MHz, DMSO-d_6, δ in ppm): 0.87 (m, 3H), 1.11 (m, 2H), 1.21 and 1.62 (m, 2H), 1.62 (m, 2H), 2.09 (m, 2H), 4.4(m, 7H_{NH}).

Cell Culture and Cell Proliferation Assay

The human breast cancer cell line of MCF-7 was received from the Pasteur Institute of Iran. Growth of cells was done on the DMEM medium (Sigma) supplemented with 2 mM L-glutamine, streptomycin, 5 ppm penicillin, and 10% heat-inactivated fetal calf serum at 37 °C under 50%:95% CO_2:air atmosphere. The cytotoxicity activity of the newly synthesized complex was studied by MTT assay. The harvested cancer cells of MCF-7 were incubated with various sterilized concentrations of *cis*-$[Pt(NH_3)_2(isopentylgly)]NO_3$ (0–800 μM) for 24 h. IC_{50} value was determined according to the method published in Ref [20].

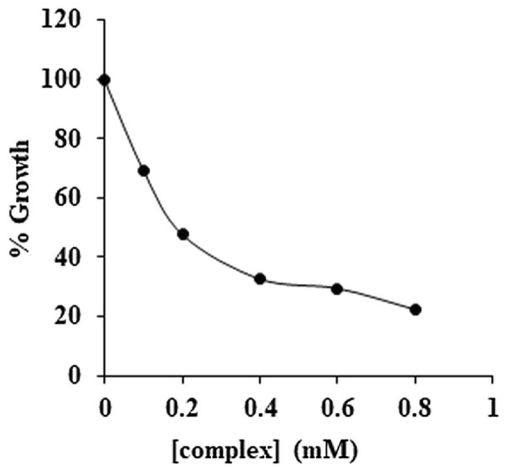

Fig. 1 Toxicity of the Pt complex against incubated MCF-7 cell lines with various concentrations of the Pt complex for 24 h

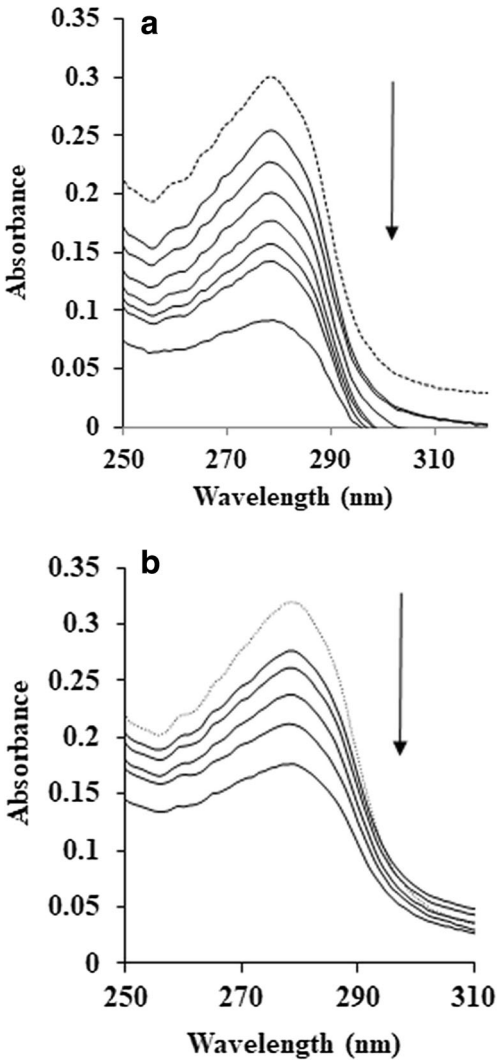

Fig. 2 Absorption spectra of HSA (15 μM) with addition of *cis*-$[Pt(NH_3)_2(isopentylgly)]NO_3$ in tris-buffer HCl-10 mM NaCl (pH = 7.4) at 27 (**a**) and 37 °C (**b**) in the absence (…) and presence (__) of this complex. The arrow shows the absorption trend with increasing concentration of the cis-$[Pt(NH_3)_2(isopentylgly)]NO_3$ complex from 0 to 228 μM

UV-Vis Spectroscopy Studies

The structural changes of HSA due to its interactions with *cis*-[Pt(NH$_3$)$_2$(isopentylgly)]NO$_3$ can be shown through UV-Vis absorption spectroscopy, which is a tool employed for studying the binding of tiny molecules to macromolecules [10].

A solution of HSA (15 μM) and Pt complex (0.8 mM) was prepared through appropriate dilution of the stock solution with tris-buffer.

The addition concentration of the *cis*-[Pt(NH$_3$)$_2$(isopentylgly)]NO$_3$ complex from 0 to 228 μM to the HSA solution were monitored by the absorption reading up until no further changes. Afterward, thermodynamic parameters such as ΔG_b° Gibbs free energy changes; ΔH_b°, the heat necessary for HSA binding without metal complex adding; ΔS_b°, the entropy of HSA binding by the complex; and the measure of the capability of the complex to binding with HSA were found using binding diagrams and the formula [21]. The spectra were taken from 200 to 700 nm in a quartz cuvette (whole cuvette volume was 1000 μL) at 27 and 37 °C.

Thermal Binding Measurements

The thermal binding experiment reveals the conformational alterations of HSA and the stability of the HSA–complex interactions [20]. This experiment was done by reading the UV-Vis absorption of HSA (7.5 μM) at pH = 7.4 at 278 nm in the presence of 0–800 μM Pt complex from 25 to 85 °C with 1 °C min^{-1}.

Kinetic Study

Knowledge about the possible mechanism of HSA interaction with Pt complex could be provided by kinetic studies [20].

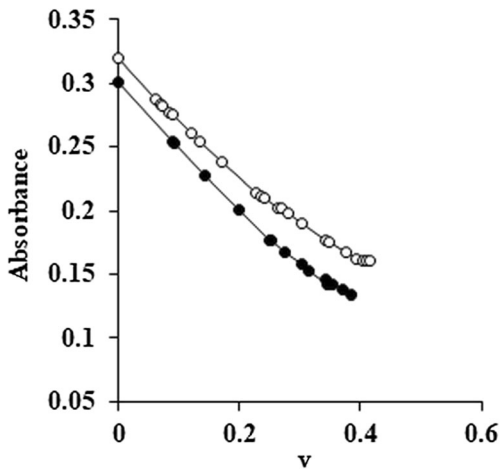

Fig. 3 HSA absorbance at 278 nm vs ν (ν = [complex]$_b$/[HSA]$_t$) at 27 (●)and 37 °C (○)

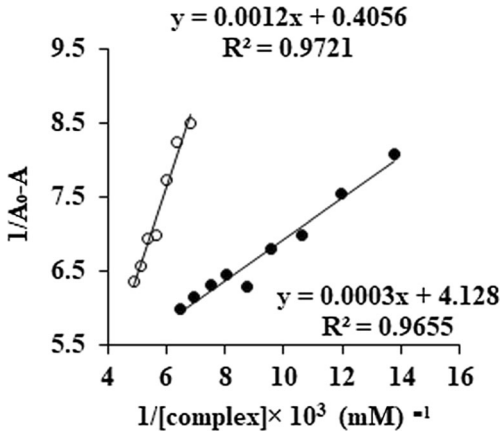

Fig. 4 The linear diagram of the reciprocal of ΔA vs the reciprocal of *cis*-[Pt(NH$_3$)$_2$(isopentylgly)]NO$_3$ at 27 (●) and 37 (○) °C

The time-scanning spectrum was 1 min at 278 nm which is λ_{max} of the Pt–HSA complex.

Fluorescence Study

The behavior of proteins as sub-target for anti-cancer metal complexes was studied via the fluorescence quenching method. Here, the fluorescence intensity changes were monitored at 280-nm excitation wavelength and within the range of 200–700-nm emission wavelengths. In each monitoring, HSA–Pt complex solutions were incubated for 5 min after the complex addition.

Molecular Docking

The 3D structure of the Pt complex was generated using the HyperChem software, and its geometry was optimized using the Gaussian 03 software by using the B3LYP method at the level of 6–31 g* [22]. Protein Data Bank (PDB) ID: 5ORI is the crystal structure of HSA in http://www.rcsb.org/pdb, which was selected in the Protein Data Bank. The *R* value (0.188 Å) and resolution of this file (1.94 Å) were prepared at pH = 7.4. Molecular docking computation was implemented by using the AutoDock 4.2 program parcel by the AutoDock tentative free energy operation and the Lamarckian genetic algorithm with a positional probe. Initially, water molecules should be removed from the initial structure of HSA and the missing hydrogen and Gasteiger charges should be set up in the HSA input file. For preparing ligand–HSA files (PDBQT), the AutoDock tools can be used. Docking imagery was considered in 80 × 80 × 80 points in a box and spacing of 0.375 Å for the Pt complex [23]. The number of docking implement of each docking simulation was adjusted to 100. As mentioned, this study

Table 1 Thermodynamic parameters and $L_{1/2}$ value of HSA binding with the platinum (II) complex

Complex	Temperature (°C)	$L_{1/2}$ (mM)	ΔG_b^* $\left(\text{kJ mol}^{(-1)}\right)$	ΔH_b^* $\left(\text{kJ mol}^{(-1)}\right)$	ΔS_b^* $\left(\text{kJ mol}^{(-1)}\text{K}^{(-1)}\right)$
cis-$[Pt(NH_3)_2(isopentylgly)]NO_3$	27	0.14	− 23.8	− 425.1	− 1.34
	37	0.11	− 15.0		

was done to investigate the binding sites on HSA for the Pt complex.

Results and Discussion

In Vitro Studies

The cytotoxicity of anti-tumor virtues of the *cis*-$[Pt(NH_3)_2(isopentylgly)]NO_3$ was checked by testing the complex against the human breast cell line of MCF-7. In this research, diverse concentrations of Pt(II) complex ranging 0–800 μM were added to the tumor cell line culture at 37 °C for 24 h. The value of 50% cytotoxic concentration (IC_{50}) of the complex was specified based on Fig. 1 and after 24-h incubation, which was determined as 175 μM for the Pt complex. For positive control, clinical anti-cancer drug such as cisplatin was used with IC_{50} equal to 80 μM which is lower than the synthesized Pt complex. The activity of the synthesized complex is less than that of cisplatin, but it is preferred because of its lower toxicity and biocompatibility. Figure 1 reveals that the cell growths after incubation time were reduced by concentration adding of the Pt complex not as good as cisplatin. Also, the water-soluble Pt(II) complex with isopentyl hydrocarbon chain could be produced with lower dosage and time–response deterrence against MCF-7 cell lines.

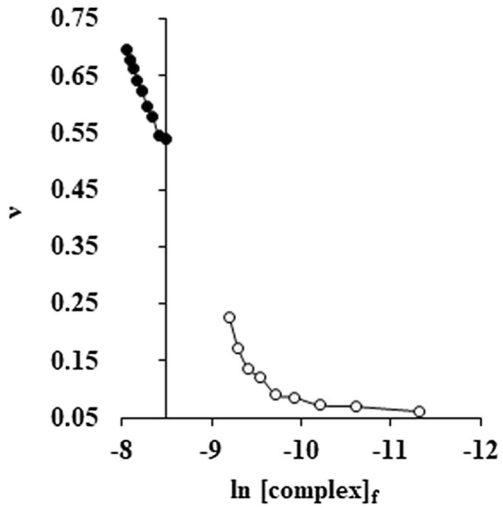

Fig. 5 The binding isotherm of HSA with the complex at 27 (●) and 37 °C (○)

HSA Binding Data and Evaluation of Thermodynamic Parameters

UV-Vis absorption study is a very practical way to study the binding of any compound to HSA. In an HSA binding exam, HSA absorption changes were reported at 278 nm by adding 10-μL stock complex solutions in each injection at both temperatures. The binding graph is shown in Fig. 2 for this

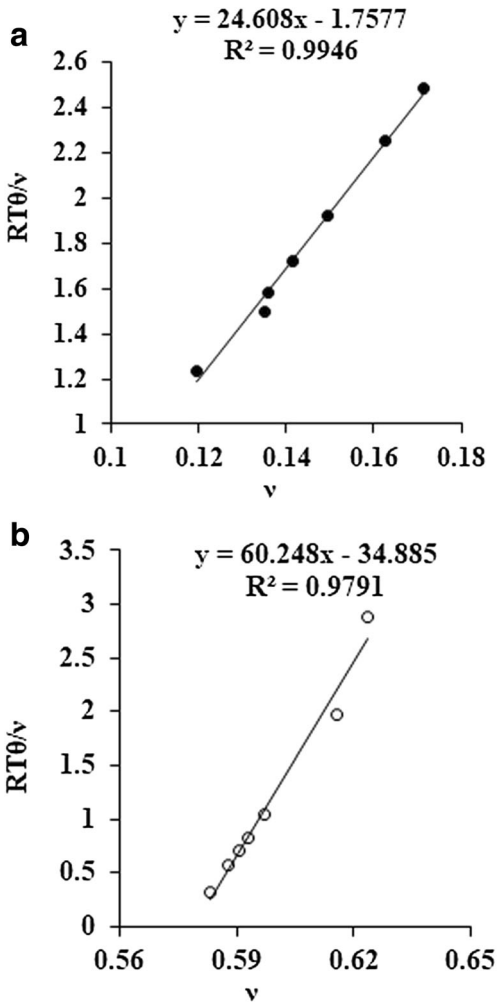

Fig. 6 The plot of $\frac{RT\theta}{\nu}$ vs ν for HSA interaction with the complex at 27 (**a**) and 37 °C (**b**)

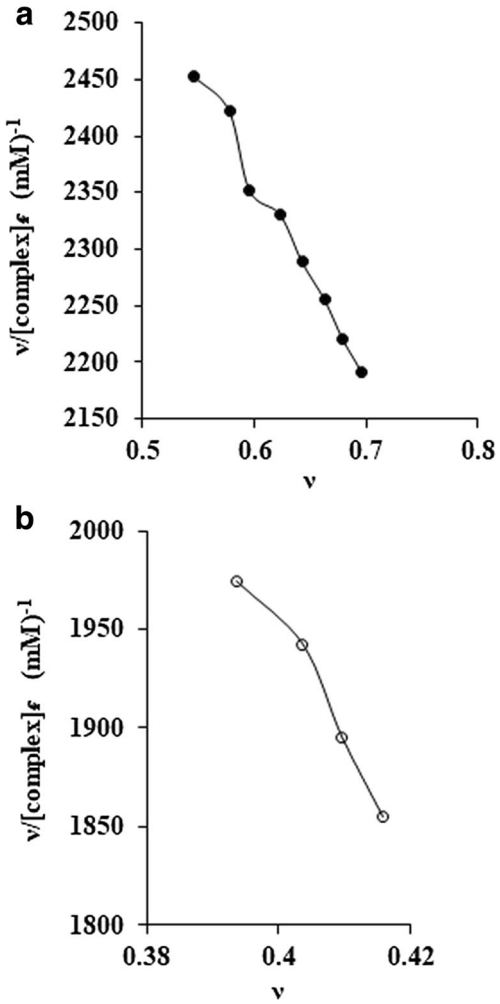

Fig. 7 Scatchard plot for HSA binding with the complex at the temperature of **a** 27 and **b** 37 °C

compound. The absorption trend in this figure shows that the absorption values diminished by adding Pt complex to free HSA meaning that HSA–Pt complex was created. The concentrations of the *cis*-[$Pt(NH_3)_2$(isopentylgly)]NO_3 in the middle of transfer the innate to bonded albumin decreased from 27 to 37 °C due to HSA-complex formation [20].

In this research, the complex could bind with HSA about 100 μM. So, this complex can be a candidate as an anti-cancer agent, whose low dosage will be used in chemotherapy, with fewer side effects. This diagram has been demonstrated in Fig. 3. The binding constant, K_b, was obtained through Eq. 1.

$$\frac{1}{A-A_0}=\frac{1}{A_{\infty}-A_0}+\frac{1}{K_b[A_{\infty}-A_0]}\cdot\frac{1}{\text{complex}} \tag{1}$$

In this formula, A_0 is the primary absorption of free HSA at 278 nm without metal complex. A_∞ is the final absorption of HSA, and A denotes the absorption reading at variant concentrations of the Pt complex.

The binding constant (K_b) can be computed through the intercept to the gradient from the linear curve of $\frac{1}{A-A_0}$ vs $\frac{1}{[\text{complex}]}$ [24]. This diagram has been demonstrated in Fig. 4. In this equation, K_b is the apparent binding constant, K_{app} (a macroscopic property).

Also, the computed thermodynamic parameters of the binding of HSA with Pt complex have been determined and presented in Table 1. The K_b value, binding constant, ΔG_b°, Gibbs free energy of HSA, and the structural stability of HSA in the presence of Pt complex as well as entropy variations $\left(\Delta S_b^{\circ}\right)$ have been obtained within the range of 27 to 37 °C.

Commonly, tiny complex molecules could bind to the protein via feeble interactions mostly including hydrogen bonds, van der Waals forces, hydrophobic, and electrostatic interactions. The binding kind can be specified by the above-mentioned parameters. From the thermodynamic point of view, $\Delta H^{\circ}>0$ and $\Delta S^{\circ}>0$ show a hydrophobic interaction. Also, $\Delta H^{\circ}<0$ and $\Delta S^{\circ}<0$ indicate the formation of van der Waals force or hydrogen bond, and finally $\Delta H^{\circ}\approx 0$ and $\Delta S^{\circ}>0$ reflect an electrostatic force. These thermodynamic parameters are obtained using the Van't Hoff equation:

$$\ln\frac{K_2}{K_1}=-\frac{\Delta H^{\circ}}{R}\left(\frac{1}{T_2}-\frac{1}{T_1}\right) \tag{2}$$

$$\Delta G_b^{\circ}=\Delta H_b^{\circ}-T\Delta S_b^{\circ}=-RT\,1nK_b \tag{3}$$

where K_i is the binding constant at T_i temperature; K_b denotes the equivalency binding constant, which is identical to the effective equivalency constants, K_a; and R value is the gas constant. Thus, the negative values of ΔG_b° complex suggest that the protein binding procedure is spontaneous. The negative ΔH_b° and negative ΔS_b° values of this complex indicate that hydrogen bonds played the dominant role in the complex–HSA interaction [25].

Binding Isotherm

The binding isotherm curve was obtained for the interaction of HSA with *cis*-[$Pt(NH_3)_2$(isopentylgly)]NO_3 at 27 and 37 °C and is shown in Fig. 5. The ligand can alter the protein structure after binding, which is known as the allosteric effect. Due to the binding isotherm of oxygen to hemoglobin, these curves were determined to exist one binding set with allosteric effect in the binding of HSA with the Pt complex. This kind of binding causes positive cooperativity [26, 27].

Using Eq. 4 and chain rule in the derivative process, the binding capacity leads to the Eq. 5,

$$\theta=\left(\frac{\partial\nu}{\partial\mu_i}\right)_{T,P,\mu_{J\neq I}}=\left(\frac{\partial\nu}{RT\partial ln[\text{complex}]_f}\right)_{T,P,\mu_{J\neq I}} \tag{4}$$

Table 2 Hill parameter and binding constant of HSA interaction with the complex

Complex	Temperature (°C)	g	$K_b(M^{-1})$	$K_H(M^{-1})$	n_H
cis-[Pt(NH_3)$_2$(isopentylgly)]NO_3	27	1.9	1.4×10^4	1.9×10^3	1.2
	37	0.7	3.4×10^2	5.3×10^3	1.3

$$\theta = \frac{n_H \nu (g-\nu)}{gRT} \tag{5}$$

and by operation of maximum criterion, it can be displayed by:

$$\nu_{\max} = \frac{g}{2} \tag{6}$$

$$\frac{RT\theta}{\nu} = n_H - \frac{n_H \nu}{g} \tag{7}$$

According to Eqs. 5 and 7, the plot of $\frac{RT\theta}{\nu}$ vs ν for a system should be linear (Fig. 6) with g identical and dependent binding sites [26].

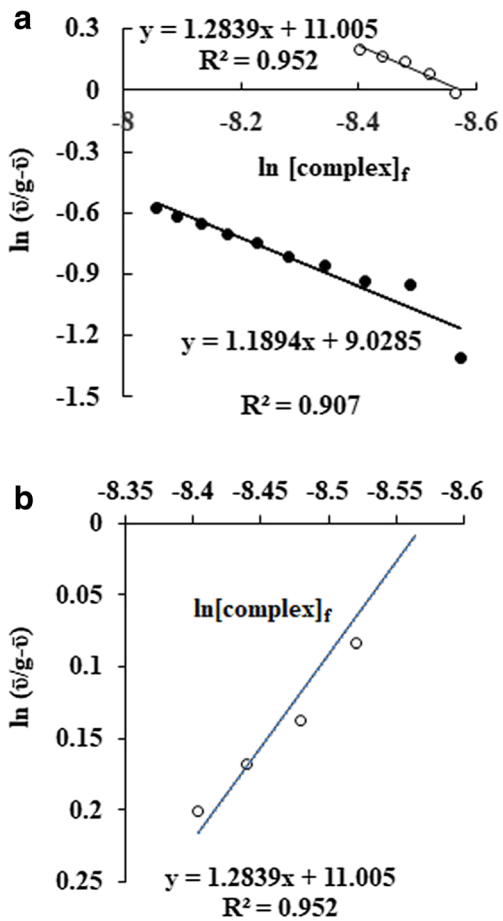

Fig. 8 Hill plot of HSA binding with the complex at the temperature of **a** 27 and **b** 37 °C

Scatchard Plot on the Interaction of HSA with *cis*-[Pt(NH_3)$_2$(Isopentylgly)]NO_3

The Scatchard equation has been shown below: [28]

$$\frac{\nu}{[\text{complex}]_f} = K^{\circ}(g-\nu) \tag{8}$$

The Scatchard diagrams of HSA binding with the complex were plotted by $\frac{\nu}{[\text{complex}]_f}$ vs ν, at both temperatures, where $\nu = \frac{[\text{complex}]}{[\text{HSA}]}$ (see Fig. 7) [28].

If the set of sites is the same and independent, the Scatchard diagram is linear, while if the set of the binding site is non-identical and dependent, the Scatchard diagram is non-linear (peak or valley) [29].

According to Fig. 7, the binding between the Pt complex and HSA is cooperative, i.e., each connection can improve the next connection. The number of the binding site (g) of the Pt complex on HSA can be obtained from the Scatchard equation.

In the same way, Hill equations have been shown further: [28]

$$ln\left(\frac{\nu}{g-\nu}\right) = lnK_H + n_H ln[\text{complex}] \tag{9}$$

For a system with a single binding set for such a system, all of the binding sites can be related to a single collection. The binding information of this system can be obtained according to the experiential Hill equation:

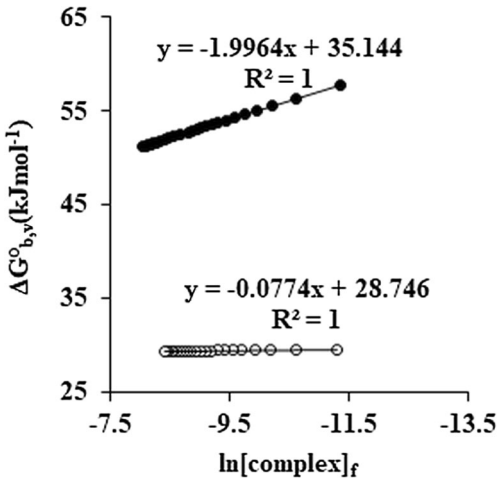

Fig. 9 The variation of $\Delta G^{\circ}_{b,\nu}$ vs ln[complex]$_f$ for HSA interaction with the complex at 27 (●) and 37 °C (○)

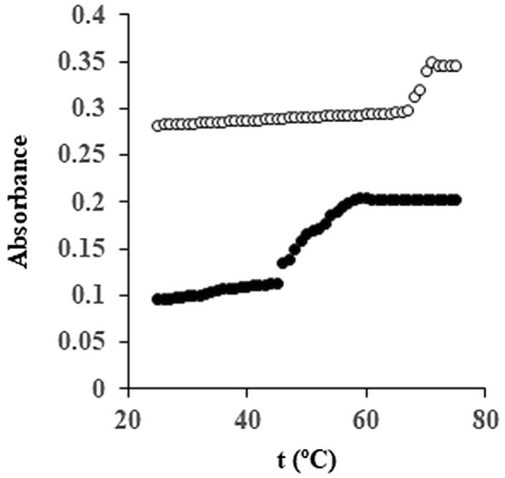

Fig. 10 Melting curve of HSA stability study without (●) and with addition (○) of *cis*-[$Pt(NH_3)_2$(isopentylgly)]NO_3 in tris-buffer

$$\nu = \frac{g\left(K_H[\text{complex}]_f\right)}{1 + \left(K[\text{complex}_f\right)^{n_H} n_H} \tag{10}$$

This can appear in the logarithmic form as follows:

$$ln\left(\frac{\nu}{g-\nu}\right) = n_H + lnK_H + n_H ln[\text{complex}]_f \tag{11}$$

Here, the binding component as Hill coefficient (n_H), the number of binding positions on the HSA molecule (g), and Hill binding constant K_H were achieved through fitting the empirical data (ν and $[\text{complex}]_f$) over the Hill equation at 27 and 37 °C (see Table 2) [28]. The Hill diagram has been shown in Fig. 8, and the results are summarized in Table 2.

The intrinsic Gibbs energy of binding per mol of the Pt complex, ΔG_b°, can be obtained by using the following equations:

$$\Delta G_b^\circ = -RTn_H lnK_H + RT(1-n_H) ln[\text{complex}]_f \tag{12}$$

Figure 9 reveals the variation of ΔG_b° vs $\ln[\text{complex}]_f$ for the interaction of the Pt complex with HSA at various concentrations of this complex. Finally, we can infer that all of the binding processes show positive cooperativity in the binding set [27].

Thermal Stability of HSA

The thermal binding empirically provides data about the stability structure of HSA with metal complex addition [30]. The melting temperature (T_m) was specified based on the transition midpoint of thermal binding diagrams of HSA [31]. ΔT_m was defined as the difference between the T_m of free HSA and the T_m of the HSA–complex. Figure 10 shows the melting plots of the HSA solutions in the absence and presence of this complex. T_m values were defined 52 and 68 °C at the ratio of R = [complex]/[HSA] 60 μL for *cis*-[$Pt(NH_3)_2$(isopentylgly)]NO_3. Thus, the stability of HSA is larger in the presence of this complex.

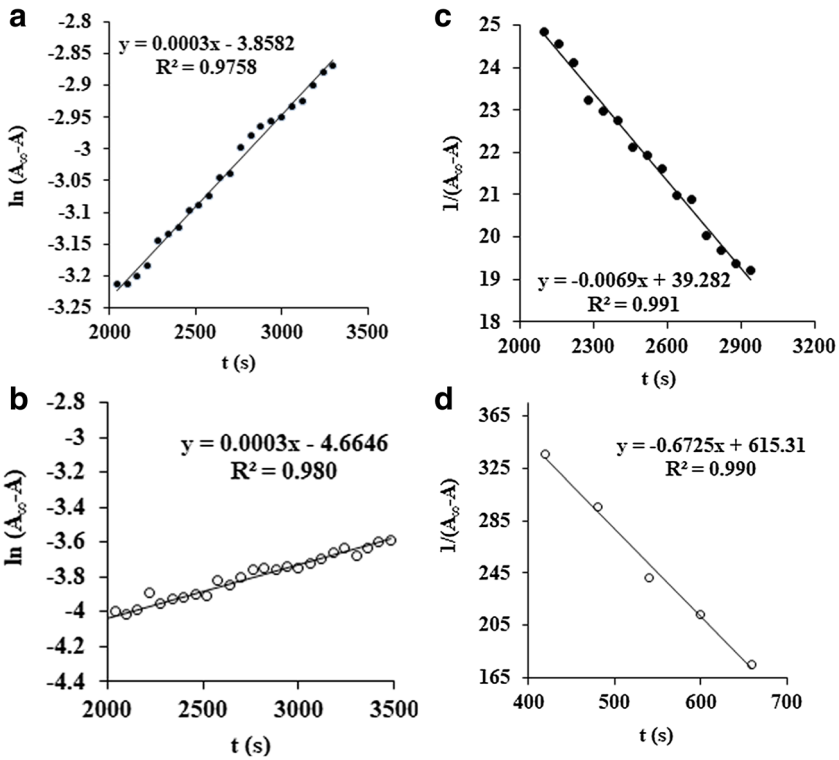

Fig. 11 The plot of **a**, **b** $\ln(A_\infty - A)$ and **c**, **d** $\frac{1}{A_\infty - A}$ vs time(s) for HSA–complex interaction at 27 (●)and 37 °C (○)

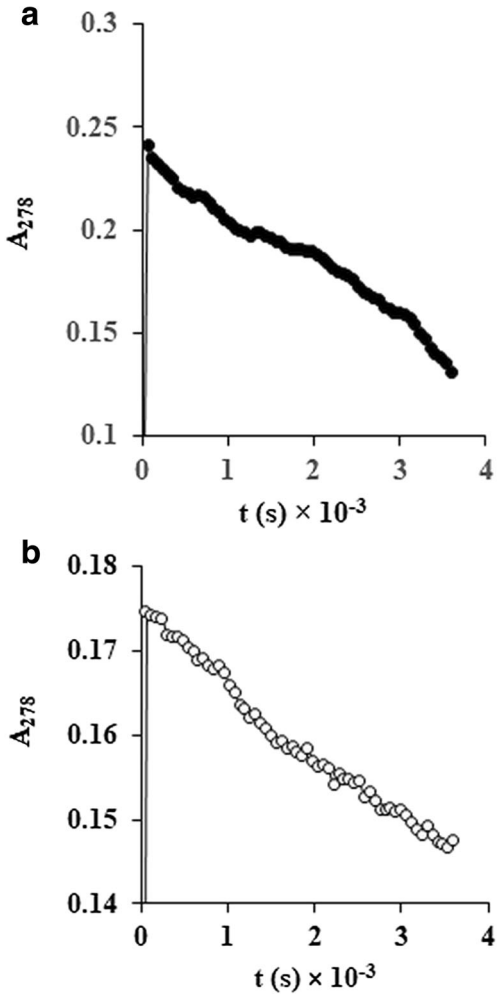

Fig. 12 Time-scanning of HSA solution in the presence of complex at ri: $\frac{[complex]}{[HSA]} = 10.64$ at **a** 27 °C and **b** 37 °C

Kinetic Study

The rate of the interaction of HSA with the complex is obtained in Eqs. 13 and 14.

$$1n(A_{\circ\circ}-A) = -ak_1t + 1n(A_{\circ\circ}-A) \tag{13}$$

$$\frac{1}{A_\infty - A} = \frac{ak_2t}{A_\infty - A} + \frac{1}{A_\infty - A_0} \tag{14}$$

In this work, the time spent on scanning was 1 h; then, concerning R, the graphs $\ln(A_\infty - A)$ vs time(s) and $\frac{1}{A_\infty - A}$ vs time(s) at 27 and 37 °C were obtained. Based on the graphs, it was found that the kinetics is a quadratic reaction (Fig. 11).

Absorption vs time diagram at 27 and 37 °C has been drawn in Fig. 12, indicating that initially, absorption is high and then becomes constant since incubation is complete [17].

Fluorescence Titration Studies

Fluorescence spectroscopy is widely used to gather information about HSA–complex interaction [32]. The innate fluorescence emission of (tryptophan, tyrosine, and phenylalanine) an HSA is a substantial participant [33]. A metal complex can quench the fluorescence emission of HSA (Fig. 13) [34].

Typically, mechanisms of fluorescence quenching can occur via static or dynamic quenching [35]. The static and dynamic mechanisms are due to the HSA–complex formation where the quencher is complex and collision between protein and the quencher, respectively [36, 37].

The Stern–Volmer equation can be used for determining quenching data.

$$\frac{F_0}{F} = 1 + K_{sv}[Q] \tag{15}$$

In this regard, $[Q]$ denotes the concentration of the Pt complex (quencher), and F_0 and F are recognized as HSA fluorescence intensities without and with Pt complex as a quencher, respectively, with the Stern–Volmer quenching constant, K_{sv}, obtained with the gradient of diagram F_0/F vs $[Q]$ (insert in Fig. 13) [4].

As inserted shown in Fig. 13, the F_0/F values vs Pt complex concentration are linear with a quenching constant from

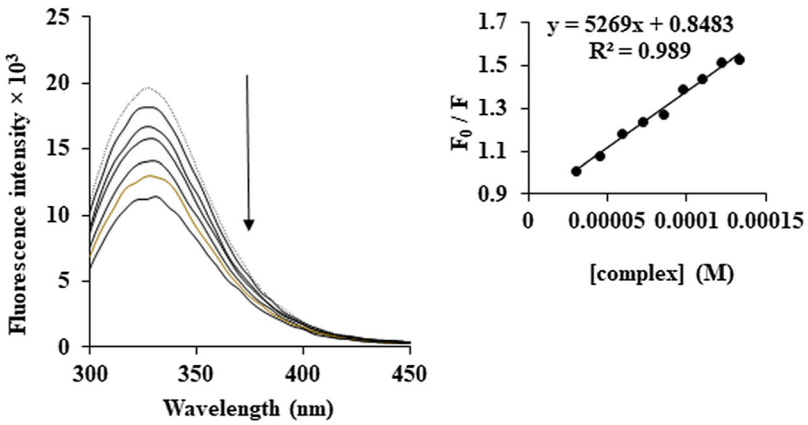

Fig. 13 The quenching intensity of HSA ($\lambda_{ex} = 280$ nm), with complex. In the insert: the Stern–Volmer plot of HSA quenching by the metal complex. The arrow shows the intensity trend with increasing concentration of the cis-$[Pt(NH_3)_2(isopentylgly)]NO_3$ complex from 0 to 180 μM

Table 3 The quenching and binding data of HSA–complex formation

Complex	$K_{SV}(M)^{-1}$	$k_q(Ms)^{-1}$	R^2	$K_b(M)^{-1}$	n	R^2	$\langle J \rangle$	R^2
cis-[Pt(NH_3)$_2$(isopentylgly)]NO_3	5.3×10^3	5.3×10^{11}	0.99	3.9×10^5	1.5	0.98	0.01	0.98

the rank 10^3 M^{-1} The linear Stern–Volmer curve shows that only one type of quenching can occur, either static or dynamic quenching [38, 39]. Using the equation of $K_{sv} = k_q\tau_0$, the mechanism of quenching can be found by the bimolecular quenching steady (k_q) and the lifetime of the chromophore (τ_0) without any quenchers, 10^{-8} s for the Pt complex–HSA [40].

The value of k_q was from the rank 10^{11} M^{-1} s^{-1} which is greater than 2×10^{10} M^{-1} s^{-1} that is maximal dynamic quenching constant[1], thus the quenching mechanism is static [41]. For static quenching, the binding constant K_b and the binding site, g, can be obtained from the following equation [42].

$$\log\left(\frac{F_0 - F}{F}\right) = \log K_b + g\log[Q] \tag{16}$$

where F_0 and F represent the quencher intensities with and without the complex, respectively. The binding data are listed in Table 3.

The calculated binding constant indicated the high binding affinity of the Pt complex towards HSA [43]. The K_b value is important for exploring the delivery of drugs, metabolism, and distribution. In public, the reduction of K_b leads to increased free medicine concentration in the plasma. Generally, a big binding constant lowers the concentration of free drug in the plasma and further improves pharmacological effects [44].

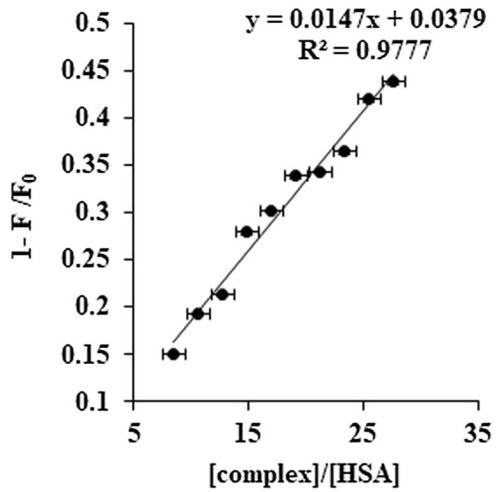

Fig. 14 The average aggregation number of HSA (<J>) with *cis*-[Pt(NH_3)$_2$(isopentylgly)]NO_3 addition. $\lambda_{ex} = 280$ nm, $\lambda_{em} = 590$ nm, and spectral bandwidth are 5 nm for both excitation and emission slits

The aggregation number of serum albumin, <J>, induced by the complex can be obtained using Eq. 17.

$$1-(F/F_0) = \langle J \rangle [Q]/[protein]_0 \tag{17}$$

The slope (<J>) of the line was determined less than one for this complex (Table 3).

This value suggests that complex binding did not cause any aggregation between albumin molecules and showed 1:1 stoichiometry for Pt(II)–serum albumin system [45]. Diagram $1 - (F/F_0)$ vs $[Q]/[\text{protein}]_0$ is displayed in Fig. 14.

Molecular Docking

Removal of water molecules from the 5ORI PDB file and missing hydrogen atoms and Gasteiger charges addition were done. Flexible-ligand docking was accomplished by using AutoDock 4.2 (http://autodock.scripps.edu) by employing empirical free energy function and the Lamarckian Genetic Algorithm, with the Auto Grid used to estimate the grids. A blind docking with 126 lattice points along three axes was done to understand the binding site of the Pt complex with the HSA. After estimates of the binding site, the dimensions of the grid map were adjusted as 80 points on a side with a grid point spacing of 0.375 Å, to allow the ligand to rotate freely. Each run of 100 docking runs was evaluated with 25,000,000 energy. The binding site of the Pt complex is shown in Fig. 15 [46, 47].

The complex bound on HSA occurred in subdomain IIA in domain I. The obtained energy of the lowest conformational energy for this complex was − 16.0 kcal mol^{-1}. Molecular docking results revealed that the prevailing forces for binding between HSA and Pt complex were hydrogen bonding and hydrophobic interactions. The amino acids involved in the hydrogen binding process for HSA–complex interaction include His3, His9, and Asp13. Also, the amino acid involved in the hydrophobic binding process for this interaction is Asp254. Figure 16 displays molecular docking analysis by using AutoDock Tools and LIGPLOT.

Conclusions

In this research, a new anti-cancer agent as such *cis*-[Pt(NH_3)$_2$(isopentylgly)]NO_3 has been synthesized

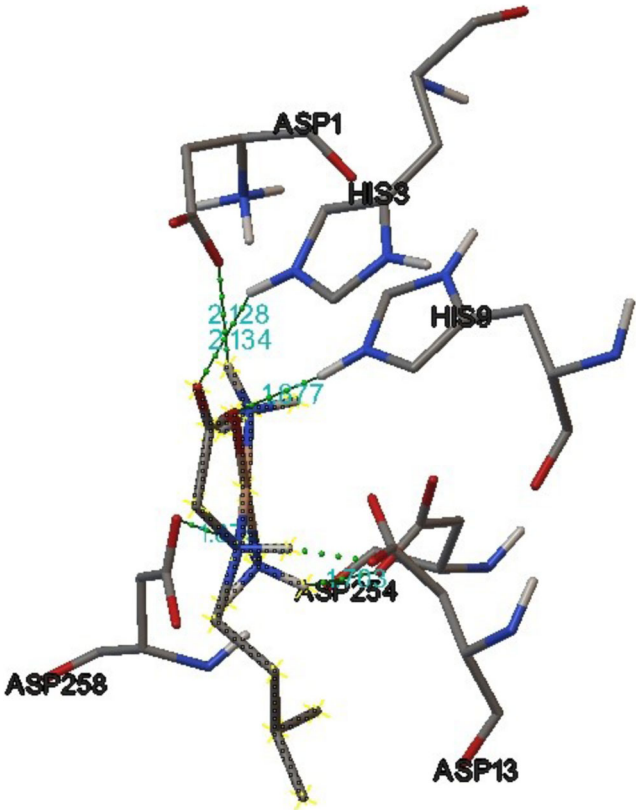

Fig. 15 Docking site of the most negative cluster in the complex–HSA system and amino acid residues surrounding the Pt complex

and specified by using spectroscopic methods. The IC_{50} of the Pt complex against the MCF-7 cell line was 175 μL, which is higher than that for cisplatin with $IC_{50} = 80\mu M$. Then, the interaction of HSA with this complex was investigated by using molecular docking and

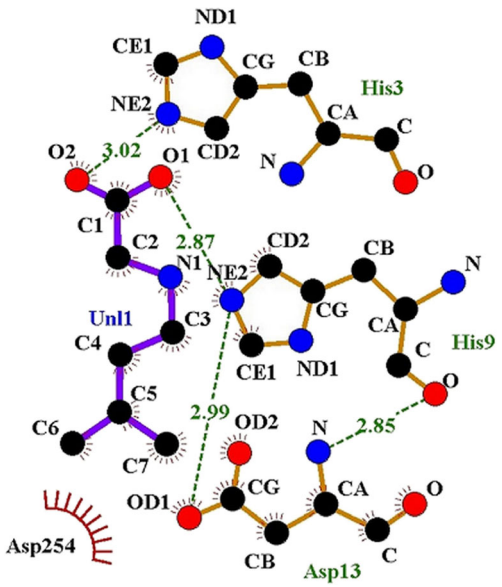

Fig. 16 Two-dimensional interactions between the complex and HSA generated by LIGPLOT

spectroscopic methods under simulated physiological conditions. The results show that the fluorescence intensity of HSA is quenched by adding the Pt complex. This interaction occurred through a static mechanism. Based on the Stern–Volmer equation, 5.3×10^3 mol^{-1} value was obtained as the binding constant. Also, the negative value of ΔH_b°, ΔG_b°, and ΔS_b° displayed the spontaneous process via hydrogen bonds. Given the allosteric effect, the Hill coefficient greater than one, the positive slope of the ΔG_b° diagram in terms of $\ln[\text{complex}]_f$, and the Scatchard diagram, this interaction has positive cooperativity. The results of the current study suggest that one complex can bind to each HSA molecule 1:1. Molecular docking demonstrated that the binding site is put in site I. This project data can be important in pharmacology and biochemistry fields and may help recognize the structural effect of the Pt complex on the blood protein as a target.

Acknowledgments The authors of this article would like to thank the Payame Noor University of Isfahan.

References

1. Kazemi Z, Rudbari HA, Sahihi M, Mirkhani V, Moghadam M, Tangestaninejad S, et al. Synthesis, characterization and biological application of four novel metal-Schiff base complexes derived from allylamine and their interactions with human serum albumin: experimental, molecular docking, and ONIOM computational study. J Photochem Photobiol B. 2016;162:448–62. https://doi.org/10.1016/j.jphotobiol.2016.07.003.
2. Hoang H, Manyanga F, Morakinyo MK, Pinkert V, Sarwary F, Fish DJ, et al. Effects of selective biotinylation on the thermodynamic stability of human serum albumin. J Biophys Chem. 2016;7(1):9–29. https://doi.org/10.4236/ibpc.2016.71002.
3. Topală T, Bodoki A, Oprean L, Oprean R. Bovine serum albumin interactions with metal complexes. Clujul Med. 2014;87:215–9. https://doi.org/10.15386/cjmed-357.
4. Zhu M, Cui X, Zhang S, Liu L, Han Z, Gao ZE. The structures, cytotoxicity, apoptosis and molecular docking controlled by the aliphatic chain of palladium (II) complexes. J Inorg Biochem. 2016;157:34–45. https://doi.org/10.1016/j.jinorgbio.2016.01.016.
5. Kantoury M, Eslami Moghadam M, Tarlani AA, Divsalar A. Structure effect of some new anticancer Pt (II) complexes of amino acid derivatives with small branched or linear hydrocarbon chains on their DNA interaction. Chem Boil Drug Dis. 2016;88(1):76–87. https://doi.org/10.1111/cbdd.12735.
6. Hadian Rasanani S, Eslami Moghadam M, Soleimani E, Divsalar A, Ajloo A, Tarlani A, et al. Anticancer activity of new imidazole derivative of 1R, 2R-diaminocyclohexane palladium and platinum complexes as DNA fluorescent probes. J Biomol Struct Dyn. 2018;36(12):3058–76. https://doi.org/10.1080/07391102.2017.1385538.
7. Aghaee E, Ghasemi JB, Manouchehri F, Balalaie S. Combined docking, molecular dynamics simulations and spectroscopic studies for the rational design of a dipeptide ligand for affinity chromatography separation of human serum albumin. J Mol Model. 2014;20(10):2446. https://doi.org/10.1007/s00894-014-2446-7.
8. Ajmal MR, Zaidi N, Alam P, Nusrat S, Siddiqi MK, Badr G, et al. Insight into the interaction of antitubercular and anticancer

compound clofazimine with human serum albumin: spectroscopy and molecular modeling. J Biomol Struct Dyn. 2017;35(1):46–57. https://doi.org/10.1080/07391102.2015.1132258.
9. Shamsi A, Ahmed A, Bano B. Probing the interaction of anticancer drug temsirolimus with human serum albumin: molecular docking and spectroscopic insight. J Biomol Struct Dyn. 2018;36:1479–89. https://doi.org/10.1080/07391102,2017,1326320.
10. Shen F, Liu YX, Li SM, Jiang CK, Wang BF, Xiong YH, et al. Synthesis, crystal structures, molecular docking and in vitro cytotoxicity studies of two new copper (ii) complexes: special emphasis on their binding to HSA. New J Chem. 2017;41(21):12429–41. https://doi.org/10.1039/c7nj02351k.
11. Yasmeen S. Exploring thermodynamic parameters and the binding energetics of berberine chloride to bovine serum albumin (BSA): spectroscopy, isothermal titration calorimetry, and molecular docking techniques. Thermochim Acta. 2017;655:76–86. https://doi.org/10.1016/j.tca.2017.06.010.
12. Kong L, Hu J, Qin D, Yan P. Interaction of ifosfamide-loaded superparamagnetic iron oxide nanoparticles with human serum albumin—a biophysical study. J Pharm Innov. 2015;10(1):13–20. https://doi.org/10.1007/s12247-014-9199-9.
13. Ojha H, Mishra K, Hassan MI, Chaudhury NK. Spectroscopic and isothermal titration calorimetry studies of binding interaction of ferulic acid with bovine serum albumin. Thermochim Acta. 2012;2012(548):56–64. https://doi.org/10.1016/j.tca.2012.08.016.
14. Trynda-Lemiesz L, Wiglusz K. Effects of glycation on meloxicam binding to human serum albumin. J Mol Struct. 2011;995(1–3):35–40. https://doi.org/10.1016/j.molstruc.2011.03.037.
15. Tang J, Lian N, Bi C, Li W. Analysis of eupatilin-human serum albumin interactions by means of spectroscopic and computational modeling. J Pharm Pharmacol. 2007;59(5):637–43. https://doi.org/10.1211/jpp.59.5.0003.
16. Mohammadgholi A, Leilabadi-Asl A, Divsalar A, Eslami Moghadam M. Multi-spectroscopic studies of the interaction of new synthesized platin complex with human carrier protein of serum albumin. J Biomol Struct Dyn. 2020:1–6. https://doi.org/10.1080/07391102.2020.1745690.
17. Kabir MZ, Tee WV, Mohamad SB, Alias Z, Tayyab S. Tayyab, interaction of an anticancer drug, gefitinib with human serum albumin: insights from fluorescence spectroscopy and computational modeling analysis. RSC Adv. 2016;6(94):91756–67. https://doi.org/10.1039/C6RA12019A.
18. Kandagal PB, Ashoka S, Seetharamappa J, Shaikh SMT, Jadegoud Y, Ijare OB. Study of the interaction of an anticancer drug with human and bovine serum albumin: spectroscopic approach. J Pharm Biomed. 2006;41:393–9. https://doi.org/10.1016/j.jpba.2005.11.037.
19. Abyaneh FSS, Moghadam ME, Divsalar A, Ajloo D, Sadr MH. Improving anticancer activity and solubility of cisplatin by methyl glycine and methylamine ligands against human breast adenocarcinoma cell line. Appl Biochem Biotechnol. 2018;186(2):271–91. https://doi.org/10.1007/s12010-018-2715-5.
20. Hadian Rasanani S, Eslami Moghadam M, Soleimani E, Divsalar A, Tarlani A. Improving the activity of anticancer oxalipalladium analog by the modification of oxalate group with isopentylglycine. J Coord Chem. 2017;70(22):3769–89. https://doi.org/10.1080/00958972.2017.1395417.
21. Becke AD. Density-functional thermochemistry: the role of extract exchange. J Chem Phys. 1993;98:5648–52. https://doi.org/10.1063/1.464913.
22. Francl MM, Pietro WJ, Hehre WJ, Binkley JS, Gordon MS, DeFrees DJ, et al. Self-consistent molecular orbital methods. XXIII. A polarization-type basis set for second-row elements. J Chem Phys. 1982;77(7):3654–65. https://doi.org/10.1063/1.444267.
23. Bursulaya BD, Totrov M, Abagyan R, Brooks CL. Comparative study of several algorithms for flexible ligand docking. J Comput Aid Mol Des. 2003;17(11):755–63. https://doi.org/10.1023/b:jcam.0000017496.76572.6f.
24. Heydari A, Mansouri-Torshizi H. Design, synthesis, characterization, cytotoxicity, molecular docking and analysis of binding interactions of novel acetylacetonatopalladium (II) alanine and valine complexes with CT-DNA and BSA. RSC Adv. 2016;6(98):96121–37. https://doi.org/10.1039/C6RA18803F.
25. Fu XB, Liu DD, Lin Y, Hu W, Mao ZW, Le XY. Water-soluble DNA minor groove binders as potential chemotherapeutic agents: synthesis, characterization, DNA binding and cleavage, antioxidation, cytotoxicity and HSA interactions. Dalton T. 2014;43(23):8721–37. https://doi.org/10.1039/c3dt53577k.
26. Bordbar AK, Saadati Z, Sohrabi N. Analysis of ligand binding process using the binding capacity concept. Acta Biochim Pol. 2004;51(4):963–70 10/045104963.
27. Hosseinzadeh R, Bordbar AK, Matin AA, Maleki R. Potentiometric study of cetylpyridinium chloride cooperative binding to anionic azo-dyes. J Braz Chem Soc. 2007;18(2):359–63. https://doi.org/10.1590/S0103-50532007000200017.
28. Heydari M, Moghadam ME, Tarlani A, Farhangian H. DNA as a target for anticancer phen-imidazole Pd (II) complexes. Appl Biochem Biotechnol. 2017;182(1):110–27. https://doi.org/10.1007/s12010-016-2314-2.
29. Bordbar AK, Moosavi-Movahedi AA, Amini MK. A microcalorimetry and binding study on the interaction of dodecyl trimethylammonium bromide with wigeon hemoglobin. Thermochim Acta. 2003;400(1–2):95–100. https://doi.org/10.1016/S0040-6031(02)00483-5.
30. Proetto MT, Liu W, Molchanov A, Sheldrick WS, Hagenbach AA, Abram U, et al. Synthesis, characterization, and in vitro antiproliferative activity of [salophene] platinum (II) complexes. Chem Med Chem. 2014;9(6):1176–87. https://doi.org/10.1002/cmdc.201402123.
31. Liu P, Liu J, Zhang YQ, Wu BY, Wang KZ. Synthesis, DNA binding and photocleavage, and cellular uptake of an alkyl chain-linked dinuclear ruthenium (II) complex. J Photochem Photobiol B. 2015;143:89–99. https://doi.org/10.1016/j.jphotobiol.2015.01.004.
32. Chatterjee T, Pal A, Dey S, Chatterjee BK, Chakrabarti P. Interaction of virstatin with human serum albumin: spectroscopic analysis and molecular modeling. PLoS One. 2012;7(5):e37468. https://doi.org/10.1371/journal.pone.0037468.
33. Gao D, Tian Y, Bi S, Chen Y, Yu A, Zhang H. Studies on the interaction of colloidal gold and serum albumins by spectral methods. Spectrochim Acta A. 2005;62(4–5):1203–8. https://doi.org/10.1016/j.saa.2005.04.026.
34. Gupta RK, Kumar A, Paitandi RP, Singh RS, Mukhopadhyay S, Verma SP, et al. Heteroleptic arene Ru (II) dipyrrinato complexes: DNA, protein binding and anti-cancer activity against the ACHN cancer cell line. Dalton S. 2016;45(16):7163–77. https://doi.org/10.1039/C6DT00446F.
35. Villarreal W, Colina-Vegas L, Rodrigues de Oliveira C, Tenorio JC, Ellena J, Gozzo FC, et al. Chiral platinum (II) complexes featuring phosphine and chloroquine ligands as cytotoxic and monofunctional DNA-binding agents. Inorg Chem. 2015;54:11709–20. https://doi.org/10.1021/acs.inorgchem.5b01647.
36. Divsalar A, Razmi M, Saboury AA, Mansouri-Torshizi H, Ahmad F. Biological evaluation of a new synthesized Pt (II) complex by cytotoxic and spectroscopic studies. Cell Biochem Biophys. 2015;71(3):1415–24. https://doi.org/10.1007/s12013-014-0364-z.
37. Shao J, Bao WG, Tian H, Li B, Zhao XF, Qiao X, et al. Nuclease activity and protein-binding properties of a novel tetranuclear thiosemicarbazide Pt (II) complex. Dalton T. 2014;43(4):1663–71. https://doi.org/10.1039/c3dt52044g.

38. Azimi O, Emami Z, Salari H, Chamani J. Probing the interaction of human serum albumin with norfloxacin in the presence of high-frequency electromagnetic fields: fluorescence spectroscopy and circular dichroism investigations. Molecules. 2011;16(12):9792–818. https://doi.org/10.3390/molecules16129792.
39. Guha S, Rawat SS, Chattopadhyay A, Bhattacharyya B. Tubulin conformation and dynamics: a red edge excitation shift study. Biochemistry. 1996;35(41):13426–33. https://doi.org/10.1021/bi961251g.
40. Jahanban-Esfahlan A, Panahi-Azar V, Sajedi S. Spectroscopic and molecular docking studies on the interaction between N-acetyl cysteine and bovine serum albumin. Biopolymers. 2015;103:638–45. https://doi.org/10.1002/bip.22697.
41. Zhu M, Wang L, Zhang H, Fan S, Wang Z, Li QX, et al. Interactions between tetrahydroisoindoline-1, 3-dione derivatives and human serum albumin via multiple spectroscopy techniques. Environ Sci Pollut Res. 2018;25(2018):17735–48. https://doi.org/10.1007/s11356-018-1955-9.
42. Mansouri-Torshizi H, Khosravi F, Ghahghaei A, Shahraki S, Zareian-Jahromi S. Investigation on the interaction of newly designed potential antibacterial Zn (II) complexes with CT-DNA and HAS. J Biomol Struct Dyn. 2018;36(10):2713–37. https://doi.org/10.1080/07391102.2017.1363086.
43. Xiao Y, Xu K, Wang Q, Xiong X, Huang Y, Li H. Synthesis, structure, and calf-thymus DNA binding of ternary fleroxacin–Cu (ii) complexes. RSC Adv. 2016;6(83):80286–95. https://doi.org/10.1039/C6RA18971G.
44. Esteghamat-Panah R, Farrokhpour H, Hadadzadeh H, Abyar F, Rudbari HA. An experimental and quantum chemical study on the non-covalent interactions of a cyclometallated Rh (III) complex with DNA and BSA. RSC Adv. 2016;6:23913–29. https://doi.org/10.1039/C5RA24540K.
45. Asadi Z, Mosallaei H, Sedaghat M, Yousefi R. Competitive binding affinity of two lanthanum (III) macrocycle complexes toward DNA and bovine serum albumin in water. J Iran Chem Soc. 2017;14(11):2367–85. https://doi.org/10.1007/s13738-017-1172-3.
46. Anjomshoa M, Torkzadeh-Mahani M, Sahihi M, Rizzoli C, Ansari M, Janczak J, et al. Tris-chelated complexes of nickel (II) with bipyridine derivatives: DNA binding and cleavage, BSA binding, molecular docking, and cytotoxicity. J Biomol Struct Dyn. 2019;37(15):3887–904. https://doi.org/10.1080/07391102.2018.1534700.
47. Ghosh P, Devi GP, Priya R, Amrita A, Sivaramakrishna A, Babu S, et al. Spectroscopic and in silico evaluation of the interaction of DNA with six anthraquinone derivatives. Appl Biochem Biotechnol. 2013;170:1127–37. https://doi.org/10.1007/s12010-013-0259-2.